Ultrafast Energy Transfer in FMO Trimers from the Green Bacterium *Chlorobium tepidum*†

Sergei Savikhin and Walter S. Struve*

Ames Laboratory-USDOE and Department of Chemistry, Iowa State University, Ames, Iowa 50011

Received January 14, 1994; Revised Manuscript Received July 13, 1994®

ABSTRACT: Time-resolved absorption difference profiles were obtained for FMO trimers, isolated from the green thermophilic bacterium *Chlorobium tepidum*, using one- and two-color femtosecond pump–probe techniques. Uphill and downhill energy transfers between inequivalent pigments in this antenna contribute to lifetime components that range from ~100 to ~900 fs in the isotropic absorption difference signals, depending on the pump and probe wavelengths. Vibrational thermalization of BChl *a* pigments may also influence the kinetics. The major lifetime components in the anisotropy decays at most wavelengths are 75–135 fs and 1.4–2.0 ps. The slower anisotropy decays probably stem from equilibration among equivalent, lowest-energy pigments belonging to different subunits in the trimer. The initial anisotropy $r(0)$ is appreciably larger than 0.4 at several wavelengths, but $r(t)$ typically decays to a value less than 0.4 within ~100 fs.

The bacteriochlorophyll *a*–protein antenna in green sulfur photosynthetic bacteria comprises a crystalline baseplate assembly that conveys electronic excitation from the peripheral antenna (the chlorosome) to the photochemical reaction centers (Olson, 1980a). Its basic structural unit (which is known as the FMO[1] complex after Fenna, Matthews, and Olson) is a trimer of identical folded β-sheets, each of which encloses seven BChl *a* pigments. A crystallographic study of FMO trimers isolated from the green bacterium *Prosthecochloris aestuarii* yielded the earliest structure determination for any photosynthetic pigment–protein complex (Fenna et al., 1977; Matthews & Fenna, 1980). This structure has since been refined to 1.9 Å resolution (Tronrud et al., 1986). The FMO complex from *Prosthecochloris aestuarii* remains the only bacteriochlorophyll antenna whose three-dimensional structure is well characterized.

This early work stimulated a number of spectroscopic and theoretical studies of FMO trimers. Pearlstein and Hemenger (1978) predicted the existence of resonance couplings as large as ~200 cm^{-1} between BChl *a* pigments complexed to the same protein subunit (Matthews & Fenna, 1980). Initial, unsuccessful attempts at simulating FMO trimer Q_y absorption and CD spectra (Philipson & Sauer, 1972; Olson et al., 1976) were based on the premise that negligible resonance interactions exist between pigments complexed to different subunits in a trimer (Pearlstein & Hemenger, 1978). Spectral hole-burning studies later established the presence of significant exciton couplings between chromophores in different subunits (Johnson & Small, 1991). Lu and Pearlstein (1993) subsequently achieved realistic exciton simulations of the Q_y spectra by incorporating resonance interactions among all 21 BChl *a* pigments within a trimer. These simulations yielded the significant conclusion that if all of the resonance interactions were absent, the seven distinct single-site BChl *a* Q_y transition energies (which cannot be directly measured in steady-state spectra owing to their redistribution by exciton splittings) would still be dispersed over a range of ~600 cm^{-1} (780–820 nm). This diagonal energy dispersion, which presumably arises from well-defined differences in protein environment, ligation (Matthews & Fenna, 1989), or pigment conformation (Gudowska-Nowak et al., 1990), may have important consequences for energy transfer kinetics within FMO trimers.

Very similar FMO proteins have been isolated from other green sulfur bacteria. The thermophilic green bacterium *Chlorobium tepidum* (Wahlund et al., 1991) yields FMO trimers with room temperature absorption spectra that are nearly indistinguishable from those of other FMO proteins (Blankenship et al., 1993). The FMO protein sequence from *C. tepidum* is 78% homologous to that of *P. aestuarii* (Daurat-Larroque, 1986), and all of the pigment-coordinating residues are conserved.

Few ultrafast time-resolved experiments have examined FMO trimer energy transfer kinetics, because most of the early processes in this antenna protein occur on a time scale of ≤2 ps (Lyle & Struve, 1990; Savikhin et al., 1994). One-color anisotropy decays obtained in an 814 nm pump–probe study of FMO trimers from *P. aestuarii* exhibited a 2.3 ps lifetime component, corresponding to energy transfer between BChl *a* pigments absorbing at that wavelength with contrasting transition moment directions (Lyle & Struve, 1990). The initial anisotropy, $r(0)$, in that work (performed with ~2 ps instrument function) was much lower than 0.4, suggesting that unresolved subpicosecond components contribute to the anisotropy decay. Savikhin et al. (1994) recently performed pump–probe studies on FMO trimers from *C. tepidum* with ~100 fs resolution. Biexponential fits to their anisotropy decays at 796 and 821 nm yielded components with lifetimes of ~100–130 fs and 1.7–2.0 ps. One- and two-color isotropic absorption difference signals clearly indicated that downhill energy transfers from 800 to 820 nm pigments occur on a time scale of 350–450 fs. In this paper, we have expanded these preliminary experiments by investigating more combinations of pump and probe wavelengths. These experiments reveal a broader range of subpicosecond isotropic decay kinetics (~100–900 fs) than the previous work. We discuss the

† The Ames Laboratory is operated for the U.S. Department of Energy by Iowa State University under Contract W-7405-Eng-82. This work was supported in part by the Division of Chemical Sciences, Office of Basic Energy Sciences.

® Abstract published in *Advance ACS Abstracts,* September 1, 1994.

[1] Abbreviations: BChl *a*, bacteriochlorophyll *a*; CD, circular dichroism; ESA, excited state absorption; FMO, Fenna–Matthews–Olson; GVD, group velocity dispersion; IVR, intramolecular vibrational redistribution; PB, photobleaching; SE, stimulated emission.

0006-2960/94/0433-11200$04.50/0

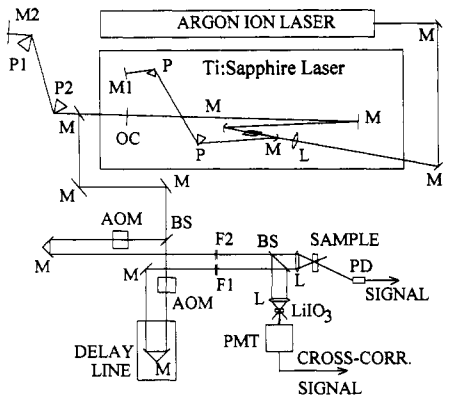

FIGURE 1: Schematic diagram of lasers and optics for two-color pump–probe experiments. In one-color experiments, the band-pass interference filters F1 and F2 are omitted, and Ti:sapphire laser tuning is achieved with an intracavity single-plate birefringent filter close to the output coupler. Generic component labels are M for dielectric mirrors, L for lenses, AOM for acousto-optic modulators, BS for beamsplitters, and P for intracavity prisms. Specific components are extracavity prisms P1, P2; photodiode PD; photomultiplier PMT; and interference band-pass filters F1, F2.

possibility that vibrational cooling and intramolecular energy redistribution (IVR) contribute to the femtosecond processes observed here. Our one- and two-color isotropic decays indicate that energy transfers among inequivalent BChl *a* pigments are responsible for much of the subpicosecond kinetics observed at some wavelengths. They also suggest that electronic excitation in FMO trimers remains at least partially delocalized for several hundred femtoseconds at room temperature. It is hoped that these results will furnish a useful data base for comparisons with energy transfer simulations in this prototypical pigment–protein complex.

MATERIALS AND METHODS

The isolation of FMO trimers from *Chlorobium tepidum* cells followed the procedure of Olson (1980b), with the modifications described by Savikhin et al. (1994). The spectral absorption ratio, defined as SAR = A_{267}/A_{371}, was 0.6 for the pure samples used here; these samples ran as a single band on SDS–PAGE. The absorption spectrum, which showed maxima at 809, 602, 371, and 267 nm, with absorbance ratios 5.4:1:2.6:1.6, was essentially congruent with those of BChl *a* proteins isolated from other green sulfur bacteria (Blankenship et al., 1993).

The self-mode-locked Ti:sapphire laser, shown in Figure 1, was a variation on the design of Huang et al. (1992). A Coherent Innova 90–5 5W multiline Ar^+ ion laser pumped a 9 mm Ti:sapphire laser rod, yielding output pulses whose durations were optimized using intracavity LaKL21 glass prisms (labeled P in Figure 1). In one-color pump–probe experiments, an intracavity single-plate birefringent filter tuned the laser output, producing a ~120 fs autocorrelation width (~80 fs laser pulse width) with a 10–12 nm spectral bandwidth for center wavelengths between 770 and 830 nm. Employing these pulses without modification in one-color experiments typically resulted in ~260 fs fwhm instrument function, due to subsequent group velocity dispersion (GVD) in the pump–probe optics (see below). In some one-color experiments, this GVD was precompensated by extracavity SF-10 glass prisms P1 and P2 separated by 50 cm, sharpening the instrument function to ~120 fs fwhm. In other one-color experiments, uncompensated pulses were deliberately used in order to separate the FMO protein molecular response signal

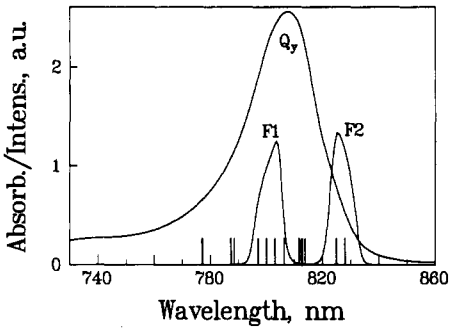

FIGURE 2: Room temperature Q_y absorption spectra of FMO trimers from *Chlorobium tepidum*, and laser pulse spectra transmitted by typical band-pass interference filters F1 and F2 in a two-color experiment (pump 800 nm, probe 830 nm). Vertical lines give center wavelengths for Q_y exciton transitions, derived from fits of model exciton calculations (Lu & Pearlstein, 1993) to absorption and Q_y spectra of FMO trimers from *Prosthecochloris aestuarii* (Olson et al., 1976).

at early times from the coherent coupling artifact (Vardeny & Tauc, 1981; Heinz et al., 1984; Palfrey & Heinz, 1985).

In two-color experiments, the intracavity birefringent filter was omitted, yielding ~40 fs fwhm laser pulses (~60 fs autocorrelation) with ~20 nm spectral bandwidth. The pump and probe pulse spectra were tailored using interference band-pass filters F1, F2 (CVI Corp.) centered at the selected pump and probe wavelengths. The transmitted spectral bandwidths were typically ~7 nm fwhm. In this inherently jitter-free two-color technique, the laser cross-correlation was typically 210 fs fwhm. In both the one- and two-color experiments, the spectrally broad femtosecond pulses typically overlapped ≥3 exciton components in the FMO trimers (Lu & Pearlstein, 1993), as shown in Figure 2.

The pump and probe beams (76 MHz repetition rate) were modulated at 6.5 and 0.5 MHz respectively in Intra-Action AOM-80NR flint glass acoustooptic modulators (AOMs). The 7.0 MHz sum frequency component in the absorption difference signal was detected with an EG&G FOD-100 Si photodiode, and directed to a modified Drake R-7A narrow-band radio receiver (Anfinrud & Struve, 1986). Room temperature solutions of FMO trimers (optical density ~0.3 at 809 nm) were rotated at ~1000 rpm in a 7.6 cm diameter, 0.5 mm path length centrifugal cell (Savikhin et al., 1993) that permitted rapid circulation of as little as 0.5 mL of sample. The apparatus instrument function was stored simultaneously with *every* pump–probe scan, by directing portions of the pump and probe pulses into the $LiIO_3$ nonlinear crystal (Figure 1).

RESULTS

Isotropic Decays. One-color isotropic absorption difference profiles are shown for an 8 ps time window in Figure 3 for several wavelengths from 773 to 835 nm. These profiles were obtained using extracavity GVD compensation (i.e., with transform-limited pulses entering the sample), so that the pump–probe instrument function was 120 fs fwhm. At the shortest wavelength (773 nm), the prompt signal is dominated by photobleaching and stimulated emission (PB/SE). However, this becomes supplanted by excited state absorption (ESA) within ~300 fs, and ESA dominates the signal thereafter. For the other wavelengths ($\lambda \geq 790$ nm), the signal is dominated by PB/SE at all times.

Optimized parameters from bi- and triexponential fits to these isotropic profiles are collated in Table 1. The lifetime groups in the triexponential fits include (a) a fast component

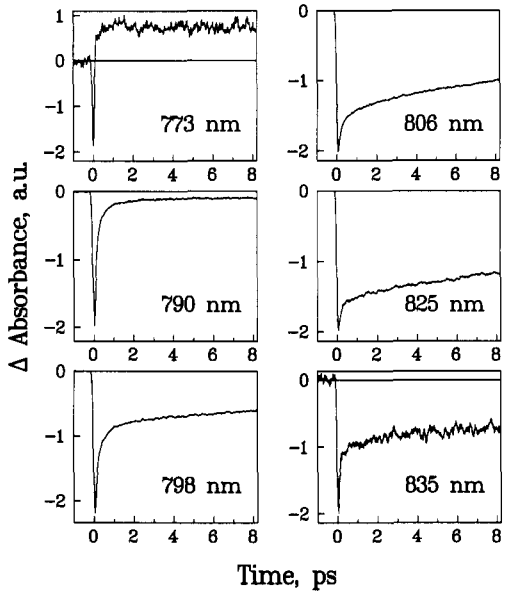

FIGURE 3: One-color isotropic absorption difference profiles for FMO trimers at several wavelengths from 773 to 835 nm. Positive and negative signals correspond to ESA and PB/SE, respectively. Table 1 gives final parameters from bi- and triexponential fits to these and other isotropic profiles.

Table 1: Optimized Bi- and Triexponential Parameters for One-Color Isotropic Absorption Difference Profiles in FMO Trimers[a]

λ, nm	window, ps	τ_1, fs (A_1)	τ_2, fs (A_2)	τ_3, ps (A_3)	χ^2 [b]
773	8	11 (–0.98)	318 (–0.02)	152 (0.06)	
790	8	58 (–0.81)	417 (–0.16)	21.8 (–0.03)	
798	8	47 (–0.64)	424 (–0.18)	25.3 (–0.18)	
806	4	18 (–0.68)	253 (–0.09)	13.3 (–0.23)	1.706
	4		123 (–0.49)	12.1 (–0.51)	2.482
806	4	23 (–0.59)	299 (–0.10)	18.8 (–0.31)	
806	8	72 (–0.41)	749 (–0.10)	24.2 (–0.48)	
815	8	64 (–0.44)		23.8 (–0.56)	
825	8	108 (–0.41)		27.6 (–0.59)	0.303
	8	28 (–0.56)	490 (–0.06)	30.5 (–0.38)	0.219
835	8	66 (–0.72)		22.8 (–0.28)	0.0934
	8	11 (–0.86)	977 (–0.04)	41.2 (–0.11)	0.0820

[a] Negative amplitudes correspond to PB/SE decay components in the absorption difference signal. [b] Unnormalized (not reduced) χ^2; meaningful comparisons of merit functions are only possible for different fits to the same experimental profile.

in the low tens of femtoseconds, (b) an intermediate 300–420 fs component at wavelengths ≤806 nm, whose lifetime increases to 490 and 980 fs at 815 and 835 nm, respectively, and (c) a slow component in the low tens of picoseconds (typically 20–30 ps). The intermediate component lifetimes are the only ones accurately measured here. The fast component lifetimes (which exhibit considerable scatter) may stem partly from optical path length differences between the pump–probe and cross-correlation measurements (10 fs = 3 μm). Wavelength variations in the empirical fast component amplitude and lifetime can also arise from the effects of pulse width, wavelength detuning, and electronic dephasing on the coherent spike (Balk & Fleming, 1985; Cong et al., 1993). For this reason, the concept of using autocorrelation traces to deconvolute absorption difference kinetics for times ≪100 fs is suspect. The optimized long component lifetimes considerably exceed our observation time windows (8 ps in some experiments, 4 ps in others); the long-time Q_y decay in FMO trimers is known to be dominated by a component with lifetime ~60 ps for FMO trimers in the absence of sodium dithionite (Blankenship et al., 1993).

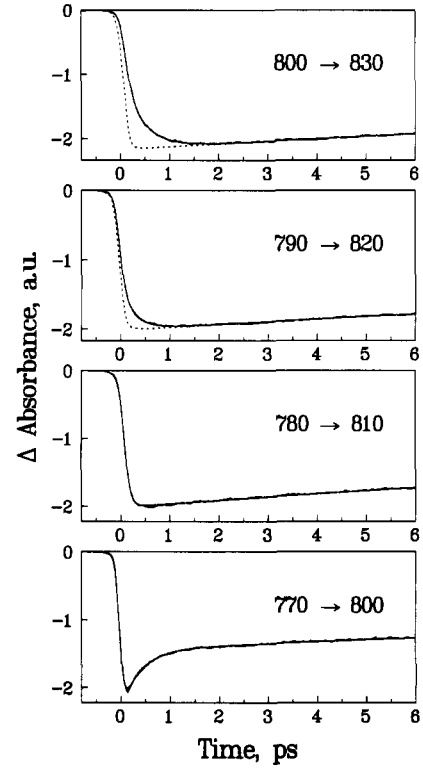

FIGURE 4: Two-color isotropic absorption difference profiles for FMO trimers, excited at a sequence of wavelengths from 800 to 770 nm. The probe wavelength in each case is 30 nm longer than the pump wavelength, so that pump and probe spectra do not overlap. Smooth continuous curves give convolutions of instrument functions with optimized triexponential models; they are nearly invisible under the experimental curves in most cases. Dashed curves are convolutions of instrument function with prompt (step-function) molecular response, and highlight the rise kinetics in the first two cases. The simulated prompt response would nearly coincide with the experimental profile in the 780→810 nm experiment.

Figure 4 shows two-color absorption difference profiles for FMO trimers excited at four wavelengths from 800 to 770 nm, and probed 30 nm to the red. These signals are dominated by PB/SE at all times. They exhibit no coherent spike, because there is no spectral overlap between pump and probe pulses. In the first case (800→830 nm), the 830 nm PB/SE signal excited at 800 nm exhibits well-defined rise behavior. A biexponential fit to this profile yields (apart from a 53.6 ps decay component similar to those in the other isotropic profiles, cf. Tables 1 and 2) a 354 fs rise component (58%) and a 42% prompt (zero-lifetime) rise component.[2] A triexponential fit to the same profile yields the rise components 159 fs (16%) and 412 fs (48%) and a prompt component (36%). The 790→820 nm profile similarly exhibits rise components, but with smaller amplitudes than in the 800→830 nm experiment. A biexponential fit in this case yields a 260 fs rise component (33%) and a prompt component (67%). However, the 780→810 nm profile in Figure 4 only exhibits minor rise components; here, a triexponential fit yields a 152 fs rise component (16%) and an 838 fs decay component (4%). The 770→800 nm profile displays no PB/SE rise behavior at all; a biexponential fit to this profile yields instead a large (38%) 405 fs *decay* component.

Figure 5 shows two-color profiles in which the probe wavelength was blue-shifted 30 nm from the pump wavelength. Clearcut PB/SE rise behavior appears in the 830→800 nm

[2] An *n*-exponential fit denotes a multiexponential fit with *n* finite-lifetime (rise plus decay) components.

Table 2: Optimized Bi- and Triexponential Parameters for Two-Color Isotropic Absorption Difference Profiles in FMO Trimers[a]

pump–probe, nm	window, ps	A_0[b]	τ_1, fs (A_1)	τ_2, fs (A_2)	τ_3, ps (A_3)	shift, fs	χ^2
800–830	8	0.36	159 (0.16)	412 (0.48)	52.5 (–1.00)	77	104
	8	0.42		354 (0.58)	53.6 (–1.00)	84	119
830–800	8	0.56	228 (0.34)	991 (0.10)	53.5 (–1.00)	120	277
	8	0.64		368 (0.36)	61.4 (–1.00)	127	369
790–820	8		67 (0.74)	348 (0.26)	47.5 (–1.00)	0[c]	785
	8	0.67		260 (0.33)	48.6 (–1.00)	67	969
780–810	8	0.87	152 (0.13)	838 (–0.04)	43.1 (–0.96)	56	461
	8	0.81	55 (0.19)		39.7 (–1.00)	53	792
	8				40.1 (–1.00)	64	897
770–800	8			405 (–0.38)	45.4 (–0.62)	–22	
810–780	8		110 (–0.65)	941 (–0.15)	27.1 (–0.19)	56	

[a] Positive and negative amplitudes correspond to PB/SE rise and decay components, respectively. The sum of amplitudes for PB/SE decay components is –1.00, while the sum of amplitudes for rise components is 1.00. [b] A_0 is the amplitude of the prompt rise component. [c] Parameter fixed.

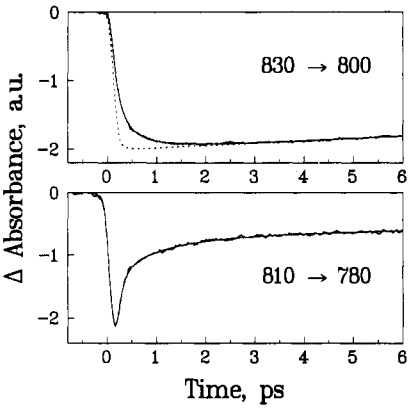

FIGURE 5: Two-color isotropic absorption difference profiles for FMO trimers excited at 830 and 810 nm. Probe wavelengths are 30 nm shorter than pump wavelengths. Multiexponential parameters for these profiles are in Table 2. The dashed curve is a simulation of prompt molecular response in the 830→800 nm experiment. Smooth continuous curves are convolutions of instrument functions with optimized triexponential decay laws (Table 2).

experiment. A biexponential fit to this profile yields a 368 fs rise component (36%) and a prompt component (64%); a triexponential fit yields 228 fs (34%) and 991 fs (10%) rise components. However, the early kinetics in the 810→780 nm profile are dominated instead by femtosecond PB/SE *decay* components with lifetimes 110 fs (65%) and 941 fs (15%).

The relative amplitude of the intermediate-lifetime PB/SE decay component in the one-color profiles of Figure 3 is largest at the shorter wavelengths (773–798 nm), and it becomes minor at 825 nm (Table 1). However, it is not absent at 835 nm, even though the lowest-energy BChl *a* components are located at ~828 nm in FMO trimers from *P. aestuarii* (Lu & Pearlstein, 1993). The intermediate-lifetime component at this wavelength (980 fs) appears to be appreciably slower than in the 773–806 nm experiments. Earlier one-color experiments, performed with nontransform-limited pulses (Savikhin et al., 1994), yielded profiles similar to the ones in Figure 1 for wavelengths ≤806 nm. However, the 821 nm one-color profile exhibited no component with a lifetime in the hundreds of femtoseconds, unlike the 825 nm profile in Figure 1. This contrast underscores the sensitivity of the absorption difference profiles to laser pulse dispersion and bandwidth.

Anisotropy Decays. Polarized one-color absorption difference profiles are shown for 821 nm in Figure 6, along with the derived anisotropy function:

$$r(t) = \frac{\Delta A_{\parallel}(t) - \Delta A_{\perp}(t)}{\Delta A_{\parallel}(t) + 2\Delta A_{\perp}(t)} \quad (1)$$

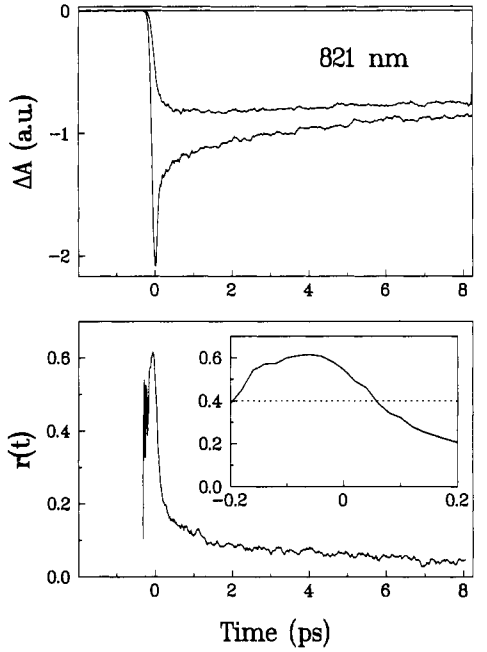

FIGURE 6: One-color anisotropic profiles and the anisotropy decay $r(t)$ for FMO trimers at 821 nm. These profiles were obtained using uncompensated laser pulses (see text). The inset shows details of $r(t)$ at early times. $\Delta A_{\perp}(t)$ and $\Delta A_{\parallel}(t)$ are given by the upper and lower curves, respectively, in the upper panel.

These profiles were obtained using nontransform-limited pulses, yielding a 260 fs fwhm instrument function. The anisotropy decay is clearly nonexponential; a biexponential fit to $r(t)$ yields component lifetimes 130 fs and 1.7 ps. The initial anisotropy $r(0)$ is nominally larger than 0.4 in Figure 6, but this conclusion must be drawn with care because the coherent spike overlaps the molecular response signal at very early times.

The relationship between the coherent spike and instrument function for laser pulses uncompensated outside of the Ti: sapphire cavity is illustrated in Figure 7, which shows the 782 nm isotropic signal for FMO trimers. At 782 nm (which is intermediate between 773 and 790 nm, wavelengths for which the asymptotic signals in Figure 3 are positive and negative, respectively), the net FMO trimer molecular response signal essentially vanishes for times >200 fs. The surviving signal is dominated by a 120 fs fwhm coherent spike, whose shape and intensity depend on the sample electronic dephasing time relative to the laser pulse width (Balk & Fleming, 1985; Cong et al., 1993). The spike in Figure 7 is superimposed on the 260 fs fwhm instrument function (the one-color autocorrelation trace) obtained without using extracavity prisms P1 and P2. The latter profile is broader than the coherent spike, due to

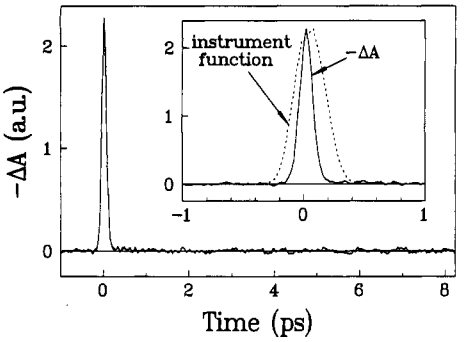

FIGURE 7: One-color isotropic profile for FMO trimers at 782 nm; the inset shows a comparison of the isotropic profile with the laser cross-correlation function on an expanded time scale. Since the GVD of laser pulses in pump–probe optics is uncompensated, the 260 fs fwhm cross-correlation function is considerably broader than the 120 fs fwhm isotropic profile.

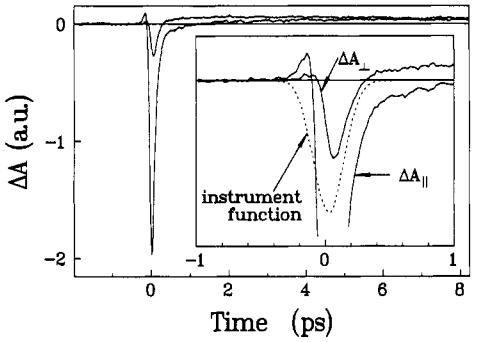

FIGURE 8: Polarized absorption difference profiles for FMO trimers at 780 nm, obtained using uncompensated laser pulses with an 8 ps time window. The inset shows the same profiles in a 2 ps time window. The 260 fs fwhm instrument function is superimposed on the inset plot.

GVD in the pump–probe optics between the Ti:sapphire output coupler and the sample cell. When the laser pulses entering the sample are made transform-limited (by including suitably spaced extracavity prisms P1 and P2), the resulting coherent spike and the autocorrelation function (not shown) nearly coincide. Deconvolution of the pump–probe signal in Figure 7 using the autocorrelation function of transform-limited pulses yields no empirical decay components with a lifetime comparable to or longer than 100 fs. Hence, the major differences between the two curves in Figure 7 arise from normal GVD in the pump–probe optics, rather than from effects of sample dephasing on the coherent spike.

While GVD broadens the instrument function, it provides leverage for separating the one-color molecular response signal at very early times from the coherent spike. Figure 8 shows the polarized absorption difference signals at 780 nm, obtained under optically dispersive conditions similar to those of Figure 7. At the earliest times (−300 to −100 fs), the pump–probe signals begin to develop concurrently with the instrument function. Since the intense coherent spike [which is prominent in $\Delta A_{\parallel}(t)$] does not set in until ~−100 fs, the pump–probe signals in this interval are essentially *pure molecular response* signals convoluted with the autocorrelation function. In this regard, they are similar to the two-color transients in Figures 4 and 5, which lack coherent spikes because their pump and probe pulse spectra do not overlap. This analogy stems from the fact that for times earlier than −100 fs, the (blue) trailing edge of the chirped probe pulse temporally overlaps the (red) leading edge of the pump pulse. Given sufficient signal/noise, these transients therefore contain meaningful information about $r(t)$ at very early times. The ratio of parallel to

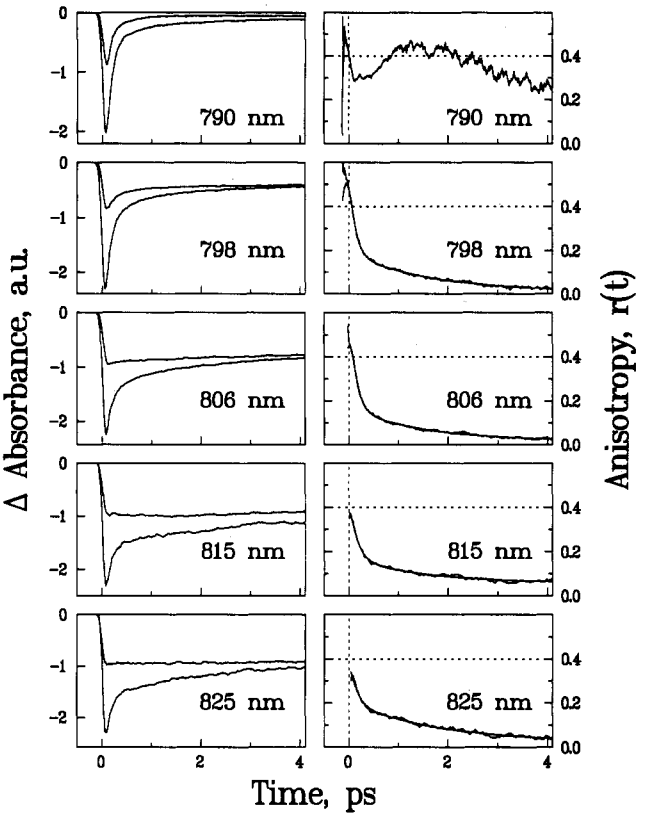

FIGURE 9: Polarized absorption difference profiles and anisotropy decay functions $r(t)$ obtained using GVD-compensated laser pulses at several wavelengths from 790 to 825 nm.

Table 3: Optimized Bi- and Triexponential Parameters for One-Color Anisotropy Decays in FMO Trimers

λ, nm	window, ps	τ_1, fs (A_1)	τ_2, ps (A_2)	τ_3, ps (A_3)	$r(\infty)$
790	8	100[a] (1.08)	0.51 (−0.71)	8.6 (0.83)	(−0.2)
790	8	100[a] (1.25)	0.40 (−0.77)	8.3 (0.76)	(−0.2)
798	4	104 (1.27)	1.49 (0.21)		0.02
798	4	77 (1.48)	1.38 (0.21)		0.02
798	8	87 (1.05)	1.73 (0.20)		0.01
806	4	78 (1.82)	0.90 (0.21)		0.04
806	4	86 (1.5)	1.10 (0.19)		0.03
806	4	103 (0.68)	0.93 (0.19)		0.04
806	8	118 (0.73)	1.43 (0.16)		0.02
815	4	92 (0.76)	0.85 (0.18)		0.07
815	4	66 (0.61)	0.82 (0.17)		0.07
815	8	134 (0.56)	1.51 (0.12)		0.06
825	4	124 (0.43)	1.55 (0.16)		0.04
825	8	90 (0.44)	1.91 (0.19)		0.02
825	8	116 (0.43)	2.00 (0.19)		0.02

[a] Parameter fixed.

perpendicular signals is clearly >3.0 [and thus $r(t) > 0.4$] at 780 nm. Close examination of the magnified anisotropy function at 821 nm for similar times (Figure 6 inset) indicates that the initial anisotropy $r(0)$ at this wavelength is at least 0.5. In this case, the apparent rise behavior in $r(t)$ at negative times is actually due to chirp sweeping between the pump and probe pulses.

One-color anisotropy decays obtained using transform-limited pulses (120 fs instrument function) are shown in Figure 9 for several wavelengths from 790 to 825 nm. With the exception of the anomalous anisotropy function at 790 nm, they are well described by biexponential models. The short component lifetime is typically 75–135 fs, while the long component lifetime depends on the time window (Table 3). Using a 4 ps window yields long component lifetimes of 0.8–1.5 ps, while profiles obtained with an 8 ps window (not shown

in Figure 9 but listed in Table 3) typically yield lifetimes of 1.4–2.0 ps. The long components obtained using the 8 ps window are likely to be more accurate, and they are similar to the 2.3 ps anisotropy decay observed at 814 nm in FMO trimers from *P. aestuarii* under lower time resolution (Lyle & Struve, 1990). The initial anisotropies $r(0)$ are not accurately determined in these one-color experiments using transform-limited pulses, because the coherent spike contributes disproportionately to $\Delta A_{\parallel}(t)$. For this reason, the optimized amplitudes in Table 3 [which should sum to $r(0)$ in the absence of coherent artifacts] often sum to numbers larger than 1.0. Such a scenario appears to be physically unlikely (see Discussion). While the zero-time extrapolations of $r(t)$ implied in Figure 9 are therefore not meaningful, this figure does show that $r(t)$ decays to ≤ 0.4 within ≤ 100 fs in all cases. The anomalous anisotropy decay at 790 nm may result from this wavelength's proximity to the zero-crossing point of the BChl *a* absorption difference spectrum, where the signal/noise ratio is low due to near-cancellation of the PB/SE and ESA signals.

DISCUSSION

Two issues arise in the interpretation of the isotropic decay kinetics (Figures 3–5 and Tables 1 and 2). The first is the extent to which vibrational cooling and IVR contribute to the intermediate-lifetime components observed in the one- and two-color experiments. Acceptor pigments contain up to ~ 750 cm^{-1} of excess vibrational energy after downhill energy transfers in FMO trimers, and their vibrational cooling (as well as vibrational cooling of Franck–Condon excited donor pigments) must contribute to the empirical "spectral equilibration" kinetics. The second issue is the persistence of exciton coherence during the first few hundreds of femtoseconds, because coherence decay is expected to influence the absorption difference spectrum of FMO trimers (van Amerongen & Struve, 1991).

Becker, Nagarajan, and Parson (1991) analyzed time-resolved absorption difference spectra of BChl *a* monomers excited in their Q_x band with 800 fs pulses. The Q_y ESA spectrum in methanol overlaps the ground state Q_y absorption spectrum; it is considerably broader than the ground state absorption spectrum, and its maximum cross section (at ~ 750 nm) is $\sim 1/2$ that of the ground state absorption spectrum ($\lambda_{max} \sim 770$ nm). The net absorption difference spectrum of BChl *a* monomers in methanol is thus dominated by ESA for wavelengths <740 nm, and by PB/SE for wavelengths between 740 and 850 nm. The Q_y PB/SE band maximum of BChl *a* monomers undergoes a dynamic Stokes shift with solvent-dependent kinetics. In pyridine, the Stokes shift was well described using a single-exponential model with 2.7 ps lifetime. Biexponential models were needed to fit the kinetics in alcohols, with lifetime components of 1.5 and 18 ps in methanol, and 1.1 and 82 ps in 1-propanol. These workers did not differentiate between dielectric relaxation and vibrational cooling as possible origins for the Stokes shifts. We have measured one- and two-color absorption difference profiles for BChl *a* monomers in 1-propanol ($\lambda_{max} = 777$ nm) using the present apparatus (S. Savikhin and W. S. Struve, unpublished work). As in FMO trimers, substantial femtosecond components arise in triexponential analyses of the absorption difference profiles of BChl *a* in 1-propanol. The fitted lifetimes depend on the time window used, indicating that the true spectral shifting kinetics are not well described by a single triexponential model. For example, analyses of 800 nm one-color profiles in 1-propanol yield PB/SE decay components with lifetimes 440 fs (23%) and 15 ps (30%) in an 8 ps window, and lifetimes 1.7 ps (18%) and 17 ps (18%) in a 24 ps window. Triexponential analysis of a 770→800 nm two-color profile in an 8 ps window yields 590 fs and 4.2 ps PB/SE rise components, while the 800→820 nm profile shows 510 fs and 11 ps PB/SE decay components. For a given probe wavelength, the two-color profiles depend on the pump wavelength, in a manner consistent with the occurrence of dynamic red-shifting in the BChl *a* PB/SE band maximum for pump wavelengths <800 nm, and blue-shifting for wavelengths on the red edge of the BChl *a* Q_y absorption band (≥ 800 nm). These observations prove that vibrational thermalization contributes to the femtosecond kinetics of BChl *a* in 1-propanol; dielectric relaxation may also play a role. Our results are not directly comparable to those of Becker et al. (1991) in the same solvent, because Q_y band excitation yields Franck–Condon vibrational distributions, while Q_x excitation leads to a Q_y state in which the accepting modes in the $Q_x \rightarrow Q_y$ internal conversion are vibrationally hot.

Vibrational cooling must therefore be considered as a possible origin of femtosecond components in the absorption difference spectroscopy of FMO trimers. (Dielectric relaxation appears unlikely to be important for BChl *a* pigments in the hydrophobic interior of folded protein β-sheets.) However, vibrational cooling and/or IVR *alone* cannot account for the major features in the 773 nm one-color profile (Figure 3), where a prompt PB/SE signal is replaced by ESA within 300 fs. The zero-crossing point between the PB/SE- and ESA-dominated regions of the BChl *a* monomer absorption difference spectrum lies ~ 50 nm to the blue of the PB/SE maximum (which is between the peak positions in the PB and SE cross sections). An upper bound for spectral shifts produced by vibrational thermalization is the separation between the excitation wavelength and the stimulated emission band maximum. For BChl *a* pigments excited near the Q_y absorption band maximum, this separation is only ~ 25 nm in the alcohols, and ~ 15 nm in pyridine (Becker et al., 1991). Hence, the bipolar switching in the 773 nm one-color profile is not primarily due to vibrational cooling. It may be explained instead in terms of energy transfers from BChl *a* pigments absorbing near 773 nm to pigments absorbing ≥ 50 nm to the red, i.e., at ≥ 825 nm. This switching qualitatively resembles the early-time behavior observed in the Chl *b* region of the LHC-II light-harvesting antenna from photosystem II (Kwa et al., 1992), which was ascribed to red-shifting of a single-site Chl absorption difference spectrum due to Chl *b* → Chl *a* energy transfers. In this context, the lack of bipolar absorption difference signals in the other one-color experiments in Figure 3 ($\lambda \geq 790$ nm) stems from the absence in FMO trimers of pigments absorbing at wavelengths much longer than ~ 825 nm. However, the femtosecond *kinetics* of the bipolar switching observed at 773 nm may be influenced by vibrational cooling (e.g., of vibrationally hot acceptor pigments) as well as by electronic energy transfer. The empirical "spectral equilibration" time scales reflected in the intermediate component lifetimes in Tables 1 and 2 are therefore only upper limits to the electronic energy transfer times.

The Q_y absorption spectrum of FMO trimers is so congested that any pump wavelength from 780 to 800 nm provides near-resonant excitation of at least one exciton component, and excites several lower-energy components as well (Figure 2). Hence, two-color profiles obtained using a fixed 30 nm separation between pump and probe wavelengths should exhibit similar subpicosecond kinetics (irrespective of pump wavelength), if the latter are dominated by donor pigment

vibrational thermalization and if all seven BChl *a* pigments in a subunit experience similar vibrational cooling kinetics. However, the 800→830 nm profile exhibits marked subpicosecond PB/SE rise kinetics, while the 780→810 nm profile does not (Figure 4 and Table 2). The two-color kinetics depend not only on the separation between pump and probe wavelengths, but also on their positions within the FMO Q_y spectrum. This suggests that energy transfers between inequivalent BChl *a* pigments (and the subsequent vibrational cooling of hot acceptor pigments) influence these femtosecond components.

In the absence of resonance couplings between chromophores, the empirical FMO absorption difference spectrum would be a weighted superimposition of BChl *a* monomer difference spectra, with their origins centered at the single-site diagonal energies. Several of the two-color profiles in Figures 4 and 5 can be rationalized in this way, using monomer difference spectra similar to the ones described by Becker et al. In this spirit, the femtosecond rise kinetics in the 800→830 nm experiment (Figure 4) can be assigned to downhill energy transfers between BChl *a* pigments absorbing near the respective wavelengths. The 830→800 nm rise kinetics (Figure 5) can similarly be attributed to uphill energy transfers, under the assumption that 830 nm prepares a distribution of states that is cooler than a Boltzmann distribution. However, the presence of femtosecond *decay* kinetics in the 770→800 nm and 810→780 nm experiments cannot be explained this way. The latter features also appear to be inconsistent with vibrational cooling alone. They suggest instead that the FMO absorption difference spectra are not combinations of monomer difference spectra, but are strongly influenced by exciton couplings. If exciton coherence persists, the absorption difference spectrum will contain (a) uniform PB of the entire FMO Q_y spectrum, regardless of which exciton component is excited; (b) SE from the exciton components that are populated; and (c) ESA due to transitions from one- to two-exciton levels (van Amerongen & Struve, 1991). The latter ESA transitions are unrelated to monomer Q_y ESA transition(s); they are inherently intense, and they overlap the Q_y spectrum that arises from the ground → one-exciton transitions. Van Amerongen and Struve (1991) have simulated prompt absorption difference spectra for the 21 pigments in an FMO trimer excited at several wavelengths in the Q_y band, using 21 and $21(21 - 1)/2 = 210$ basis functions in their expansions of one- and two-exciton states, respectively. The simulated prompt spectrum excited at 820 nm is dominated by a large PB/SE maximum between 810 and 820 nm, and exhibits a weak ESA peak at ~785 nm. However, the prompt spectrum excited at 780 nm is strongly bimodal, with PB/SE maxima (of comparable intensity) near 780 and 810 nm. This appears to be consistent with the absence of large femtosecond PB/SE rise components in the 780→810 nm two-color experiment (Figure 4). Similar mechanisms may account for the presence of PB/SE decay components observed in the 770→800 nm and 810→780 nm experiments. In these simulations, the total absorption difference spectra contain structured ESA spectra arising from one- to two-exciton transitions, and are not simply PB holes.

Some of the intermediate-lifetime components in the FMO one- and two-color profiles can be equally well explained by vibrational thermalization or electronic energy transfer. An example is the subpicosecond PB/SE decay observed in the 835 nm one-color experiment (Figure 3), where either vibrational thermalization or uphill electronic energy redistribution may cause a SE blue shift. In general, the femtosecond rise and decay features in our FMO kinetics are multiexponential, since triexponential fits yield lower χ^2 than biexponential fits (Tables 1 and 2). This is not surprising, because (a) several BChl *a* exciton components are excited at any wavelength, so that multiple energy transfer steps can contribute to any one- or two-color experiment, and (b) vibrational cooling and/or dielectric relaxation of BChl *a* is nonexponential in most solvents (Becker et al., 1991; Savikhin and Struve, unpublished work).

Table 4: Comparisons of Energy Transfer Kinetics in LHC-II and FMO Trimers

	LHC-II	FMO
anisotropy decay components	250–300 fs[a]	75–135 fs[c]
	5–12 ps[a]	1.4–2.0 ps[c]
	5–13 ps[b]	
spectral equilibration	200–300 fs[a]	350–450 fs[c,d]

[a] Du et al. (1993) (fluorescence up-conversion). [b] Kwa et al. (1992) (pump–probe). [c] This work. [d] Savikhin et al. (1994) (pump–probe).

FMO trimers bear little similarity to the LHC-II trimers that constitute the Chl *a/b* peripheral antenna in photosystem II (Kühlbrandt & Wang, 1991). Their protein conformation is different (β-sheets, versus α-helices in LHC-II trimers), and the average chromophore density (0.066 pigment/nm^3) is much lower than in LHC-II (0.18 pigment/nm^3). However, the core chromophore densities are quite similar in the two antennae (0.56 versus 0.42 pigment/nm^3). Perhaps for this reason, the lifetimes for spectral equilibration and anisotropy decays in LHC-II bear an order-of-magnitude resemblance to the lifetimes found here for FMO trimers (Table 4). The Chl *a* fluorescence anisotropies in LHC-II exhibit biexponential kinetics, with 5–12 ps and 250–300 fs components (Du et al., 1993). These are somewhat slower (by factors of 3–6) than the 1.4–2.0 ps and 75–135 fs anisotropy decay components found in FMO trimers (Table 3). LHC-II spectral equilibration components of 250–300 fs have been observed in fluorescence up-conversion experiments (Du et al., 1993). Our earlier FMO study suggested that a major time scale for spectral equilibration is 350–450 fs (Savikhin et al., 1994). The pump–probe wavelengths used in the present work reveal a considerably broader range of intermediate-lifetime components (~100–900 fs, Tables 1 and 2). Some (but certainly not all) of these components may stem from vibrational thermalization.

Multiexponential analyses of our FMO isotropic and anisotropic decays (Tables 1–3) suggest that their respective lifetime families are almost mutually exclusive, in contrast to the case for LHC-II trimers (Du et al., 1993). The 75–135 fs and 1.4–2.0 ps anisotropy components found at most wavelengths have few analogs in the isotropic decays. Most of the intermediate-lifetime isotropic components (the ones with lifetime >150 fs) are not mirrored in the anisotropy decays. In one mechanism for anisotropy decay in trimeric antenna proteins, energy transfer occurs between two pigments that belong to the same monomer and have nonparallel transition moments. Such an energy transfer would produce similar lifetime components in the resulting isotropic and anisotropy decays. In a second mechanism, excitation is equilibrated among equivalent pigments complexed to different subunits in the trimer. Such spatial (as opposed to spectral) equilibration would have no effect on the isotropic decays, but it would produce an anisotropy component with an inverse lifetime equal to 3 times the pigment-to-pigment energy transfer rate (Lyle & Struve, 1991). Since our analyses of one- and two-color isotropic decays reveal no major components

with lifetimes similar to the 1.4–2.0 ps anisotropy components, these slow anisotropy components likely stem from equilibration among equivalent (predominantly the redmost) pigments in different subunits. According to the Lu and Pearlstein simulation (1993) of absorption and CD spectra for FMO trimers from *P. aestuarii* (Olson et al., 1976), these redmost pigments are the ones denoted BChl 7, which are located in the centers of the respective BChl *a*–protein monomers (Matthews & Fenna, 1980). However, best fits of the exciton model to the Philipson and Sauer spectra (1972) suggest that the lowest-energy pigments may be BChl 3 instead (Lu & Pearlstein, 1993). The differences between the spectra of Philipson and Sauer and those of Olson et al. may arise from structural differences in the respective cryogenic solvents used (Pearlstein & Lu, 1993). While lifetimes near 2 ps have been identified with vibrational cooling and/or dielectric relaxation for BChl *a* monomers in some solvents (Becker et al., 1991), the 1.4–2.0 ps anisotropy decay components in FMO trimers *cannot* be ascribed to these processes, because these lifetimes do not turn up as major components in our analyses of their isotropic profiles.

The origin of the 75–135 fs anisotropy decay components remains uncertain. Their lifetimes are shorter than the intermediate component lifetimes in most of the isotropic decays. One possible scenario is that while the former correspond to the kinetics of energy transfers between inequivalent pigments with different orientations, the latter arise from a combination of energy transfer and vibrational cooling kinetics. Our recent experiments on BChl *a* monomers in 1-propanol show that vibrational cooling does not contribute materially to the anisotropy decays (Savikhin and Struve, unpublished work).

We finally consider the theoretical range of initial anisotropies to be expected in FMO trimers. The seven BChl *a* chromophores bound to one protein subunit give rise to seven Q_y exciton components (Pearlstein & Hemenger, 1978). In the assembled trimer, each of these seven components becomes split into a nondegenerate level and a doubly degenerate pair of levels. We denote as B_0 and (B_+, B_-) the Einstein absorption coefficients for a particular set of such sublevels, whose respective Q_y transition moments μ_0 and (μ_+, μ_-) are aligned parallel and perpendicular to the trimer symmetry axis. These three exciton transition moments are mutually perpendicular (i.e., $\mu_+ \cdot \mu_- = 0$), and the Einstein coefficients for the perpendicular exciton components are equal ($B_+ = B_-$). An extension of the Rahman, Knox, and Kenkre theory (1979) for fluorescence polarization in homodimers then leads to the expressions for the polarized photobleaching signals at zero time:

$$\Delta A_{\parallel}(0) \propto B_+^2(\mu_+\cdot x)^4 + B_0^2(\mu_0\cdot x)^4 + B_-^2(\mu_-\cdot x)^4 + 2B_+B_- (\mu_+\cdot x)^2(\mu_-\cdot x)^2 + 2B_+B_0(\mu_+\cdot x)^2(\mu_0\cdot x)^2 + 2B_-B_0(\mu_-\cdot x)^2(\mu_0\cdot x)^2 \quad (2a)$$

$$\Delta A_{\perp}(0) \propto B_+^2(\mu_+\cdot x)^2(\mu_+\cdot y)^2 + B_0^2(\mu_0\cdot x)^2(\mu_0\cdot y)^2 + B_-^2(\mu_-\cdot x)^2 (\mu_-\cdot y)^2 + 2B_+B_-(\mu_+\cdot x)(\mu_+\cdot y)(\mu_-\cdot x)(\mu_-\cdot y) + 2B_+B_0(\mu_+\cdot x) (\mu_+\cdot y)(\mu_0\cdot x)(\mu_0\cdot y) + 2B_-B_0(\mu_-\cdot x)(\mu_-\cdot y)(\mu_0\cdot x)(\mu_0\cdot y) \quad (2b)$$

in the limit where the laser output bandwidth is broad enough to uniformly excite all three exciton components (cf. Figure 2). The laboratory-fixed x- and y-directions are aligned with the parallel and perpendicular laser polarizations, respectively; the transition moment directions μ_+, μ_0, and μ_- are defined with respect to protein-fixed axes. The cross-terms proportional to B_+B_- etc. in eqs 2 arise from coherences (Cohen-Tannoudji et al., 1977; Rahman et al., 1979), which decay as a result of perturbation of the exciton levels by random protein motions. In the absence of such cross-terms, the initial anisotropy $r(0)$ evaluated from eqs 1 and 2 automatically equals 0.4, regardless of the antenna structure and laser conditions. Since the SE transition moments are essentially parallel to those for PB, the orientational factors in eqs 2 are not materially changed if SE contributes to the total absorption difference signal. It is assumed here that large ESA signals with polarization differing from that of PB are not present; pump–probe studies of BChl *a* monomers in 1-propanol (Savikhin and Struve, unpublished work) show that the Q_y ESA transition moment makes an angle of at most 20° from the ground → Q_y transition moment. Averaging the factors $(\mu_+\cdot x)^4$, etc. over the random protein orientations (Lyle & Struve, 1991) then leads to the initial anisotropy:

$$r(0) = \frac{2(B_+^2 + B_0^2 + B_-^2) + 3(B_+B_0 + B_0B_- + B_+B_-)}{5(B_+^2 + B_0^2 + B_-^2)} = \frac{7 + 2x^2 + 6x}{10 + 5x^2} \quad (3)$$

where $x \equiv B_0/B_+$. When $B_+ (=B_-) = 0$, the initial anisotropy is 0.4, as expected for a single linearly polarized electronic transition. When $x = 0$ ($B_0 = 0$, $B_+ = B_- \neq 0$), we recover the homodimer result $r(0) = 0.7$ obtained by Knox and Gülen (1993) for the circular oscillator case in which the angle between monomer transition moments is 90°. When $x = 1$ ($B_0 = B_+ = B_-$), we obtain the spherical oscillator limit $r(0) = 1.0$. Hence, $r(0)$ can vary from 0.4 to 1.0, depending on the relative dipole strengths of the exciton transitions polarized parallel and perpendicular to the trimer symmetry axis. In a real experiment, expressions like eq 3 need to be weighted over the sets of exciton levels prepared by the laser (Figure 2). The anisotropies at all wavelengths decay to values lower than 0.4 within ~100 fs (Figure 9), so that the initial coherences in the laser-excited exciton levels disappear within this time scale. Since the coherent spike in these one-color experiments is typically 120 fs fwhm, the observation of anisotropies higher than 0.4 in FMO trimers is facilitated by the deliberate use of uncompensated GVD to separate the molecular response signal from the coherence spike (cf. Figure 6).

ACKNOWLEDGMENT

We are indebted to Wenli Zhou and Robert Blankenship for the isolation of the FMO trimers. We thank the referees for many useful suggestions.

REFERENCES

Anfinrud, P., & Struve, W. S. (1986) *Rev. Sci. Instrum. 57*, 380–383.

Balk, M. W., & Fleming, G. R. (1985) *J. Chem. Phys. 83*, 4300–4307.

Becker, M., Nagarajan, V., & Parson, W. W. (1991) *J. Am. Chem. Soc. 113*, 6840–6848.

Blankenship, R. E., Cheng, P., Causgrove, T. P., Brune, D. C., Wang, S. H.-H., Choh, J.-U., & Wang, J. (1993) *Photochem. Photobiol. 57*, 103–107.

Cohen-Tannoudji, C., Diu, B., & Laloë, F. (1977) *Quantum Mechanics*, Wiley-Interscience, New York.

Cong, P., Deuel, H. P., & Simon, J. D. (1993) *Chem. Phys. Lett. 212*, 367–373.

Daurat-Larroque, S. T., Brew, K., & Fenna, R. E. (1986) *J. Biol. Chem. 261*, 3607–3615.
Dracheva, S., Williams, J. C., & Blankenship, R. E. (1992) *Research in Photosynthesis* (Murata, N., Ed) Vol. I, pp 53–56, Kluwer Academic Publishers, Dordrecht, The Netherlands.
Du, M., Xie, X., Mets, L., & Fleming, G. R. (1993) *Photochem. Photobiol. 57*, 17S.
Fenna, R. E., Ten Eyck, L. F., & Matthews, B. W. (1977) *Biochem. Biophys. Res. Commun. 75*, 751–755.
Gudowska-Nowak, E., Newton, M. D., & Fajer, J. (1990) *J. Phys. Chem. 94*, 5795–5801.
Heinz, T. F., Palfrey, S. L., & Eisenthal, K. B. (1984) *Opt. Lett. 9*, 359–361.
Huang, C. P., Asaki, M. T., Backus, S., Nathel, H., Murnane, M. M., & Kapteyn, H. C. (1992) *Opt. Lett. 17*, 1289–1292.
Johnson, S. G., & Small, G. J. (1991) *J. Phys. Chem. 95*, 471–479.
Knox, R. S., & Gülen, D. (1993) *Photochem. Photobiol. 57*, 40–43.
Kühlbrandt, W., & Wang, D. N. (1991) *Nature 350*, 130–134.
Kwa, S. L. S., van Amerongen, H., Lin, S., Dekker, J. P., van Grondelle, R., & Struve, W. S. (1992) *Biochim. Biophys. Acta 1102*, 202–212.
Lu, X., & Pearlstein, R. M. (1993) *Photochem. Photobiol. 57*, 86–91.
Lyle, P. A., & Struve, W. S. (1990) *J. Phys. Chem. 94*, 7338–7339.
Lyle, P. A., & Struve, W. S. (1991) *Photochem. Photobiol. 53*, 359–365.
Matthews, B. W., & Fenna, R. E. (1980) *Acc. Chem. Res. 13*, 309–317.
Olson, J. M. (1980a) *Biochim. Biophys. Acta* 594, 33–51.
Olson, J. M. (1980b) *Methods Enzymol. 69*, 336–344.
Olson, J. M., Ke, B., & Thompson, K. H. (1976) *Biochim. Biophys. Acta 430*, 524–537.
Palfrey, S. L., & Heinz, T. F. (1985) *J. Opt. Soc. Am. B: Opt. Phys. 2*, 674–678.
Pearlstein, R. M. (1992) *Photosynth. Res. 31*, 213–226.
Pearlstein, R. M., & Hemenger, R. P. (1978) *Proc. Natl. Acad. Sci. U.S.A.* 75, 4920–4924.
Philipson, K. D., & Sauer, K. (1972) *Biochemistry 11*, 1880–1885.
Rahman, T. S., Knox, R. S., & Kenkre, V. M. (1979) *Chem. Phys. 44*, 197–211.
Savikhin, S., Wells, T., Song, P.-S., & Struve, W. S. (1993) *Biochemistry 32*, 7512–7518.
Savikhin, S., Zhou, W., Blankenship, R. E., & Struve, W. S. (1994) *Biophys. J. 66*, 110–114.
Struve, W. S. (1994) in *Anoxygenic Photosynthetic Bacteria* (Blankenship, R. E., Madigan, M. T., & Bauer, C. E., Eds.) Kluwer Academic Publishers, Dordrecht, The Netherlands (in press).
Taguchi, A. K. W., Stocker, J. W., Alden, R. G., Causgrove, T. P., Peloquin, J. M., Boxer, S. G., & Woodbury, N. W. (1992) *Biochemistry 31*, 10345–10355.
Tronrud, D. E., Schmid, M. F., & Matthews, B. W. (1986) *J. Mol. Biol. 188*, 443–454.
Van Amerongen, H., & Struve, W. S. (1991) *J. Phys. Chem. 95*, 9020–9023.
Vardeny, Z., & Tauc, J. (1981) *Opt. Commun. 39*, 396–400.
Wahlund, T. M., Woehse, C. R., Castenholz, R. W., & Madigan, M. T. (1991) *Arch. Microbiol. 156*, 81–90.